

# Numerical Simulation of Flow Field and Proper Placement Range of an Aerosol Sampler on an UAV

Jing Zhang, Yaqin Ji \*

College of Environmental Science and Engineering  
Nankai University, Tianjin 300071, China

**Abstract**—This study has explored a method to obtain the airflow characteristics and the particle trajectories using CFD techniques and SST  $k-\omega$  around a UAV. Numerical simulations of gas-phase turbulence physics at the flight speed of 20 and 40m/s and the altitude of 600 m have been carried out. DPM model simulated the trajectories of PM<sub>1</sub>, PM<sub>2.5</sub> and PM<sub>10</sub> at different flight speed. Combined the simulation results of gas-phase and dispersed-phase, at the altitude of 600m, the optimal placement of the sampler was about 43~72 cm from the UAV nose, and the vertical distance from the X-axis must exceed 15.0cm.

**Keywords**-CFD; Numerical simulation; Optimal placement; Aerosol particles

## I INTRODUCTION

Atmospheric aerosol particles play important roles in a wide range of fields, including epidemiology, visibility degradation, and global climate change. Therefore, environmental aerosol properties have been paid considerable attention in the world [1]. Most observations were conducted at ground level or used tall buildings as platforms over scales ranging from dozens of meters to hundreds of meters [2]. Unmanned Aerial Vehicle (UAV) can detect in dangerous conditions, like high temperatures, toxic gas leaked, without a pilot. In addition, UAV can minimize the impact of the aircraft exhaust and cost-effective, it doesn't require airport when it take off.

The flow field of UAV and particles trajectories should be simulated to determine the placement of sampler. CFD has been studied extensively for the simulation of near-field pollutant dispersion in the urban environment [3,4].

The main objective of this study was to offer a methodology for determining the optimal placement of sampler outside an aircraft. Another was to provide a realistic simulation of the flow field and the distribution of particulates around the UAV using CFD.

## II NUMERICAL PROCEDURE

### A. Geometric model

The simulation used a tail-pushed fixed-wing UAV as shown in Fig.1 (a). The UAV model is perfectly symmetrical, so the half-aircraft model (Fig. 1(b)) was used to simulate. This reduced the calculation amount and the computing time.

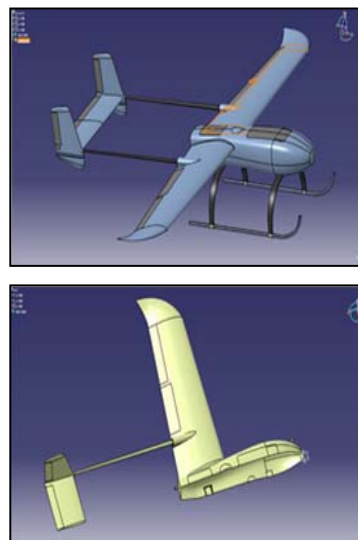


Fig.1 The geometric model of the UAV

The computational domain was set as rectangle; its length was as long as 20 times of the length of the UAV, its width and height were as long as 20 times of the wing span length. The whole model including the UAV model and the computational domain was divided into seven parts, the UAV model was defined as UAV, the six faces of the rectangle were defined as IN, OUT, UP, DOWN, SIDE, SYM (the symmetry plane of the UAV).

### B. Computational details

According to the reference [5] the unstructured mesh is the best choice to mesh a complicated 3D geometry. So in this study, the UAV model and the computational domain were meshed by unstructured meshes. The total number of meshes is 8219943.

Simulations were carried out using CFD-FLUENT software. When Mach number less than 0.3, the flight speed is considered to be low and the air to be incompressible. For this simulation, the Mach numbers were 0.059 and 0.118 for the speed of 20 and 40 m/s. So the air can be regarded as incompressible in this paper. The simulations chose the SST  $k-\omega$  model as it is more accurate and reliable for a wider class of flows (e.g., adverse-pressure-gradient flows, airfoils, transonic shock waves) than other models [6].

In the simulation the part of IN was set as velocity inlet, OUT was set as pressure outlet, DOWN, UP, SIDE were set as moving wall, the UAV was set as stationary wall.

### C. The simulation of dispersed phase

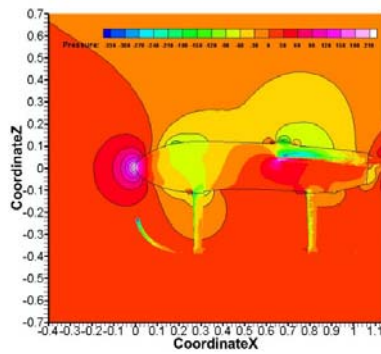
Dispersed phase model (DPM) was activated to simulate the particle trajectories after the calculation of gas-phase converged. Most researches on atmospheric particulate matter focus on three diameter: 1, 2.5, 10  $\mu\text{m}$  [7-8]. This article also chose these three diameters as the study subject. The injection type was set to group and particle type was inert. Simulations of particle released from the velocity inlet at the speed as UAV were carried out.

## III RESULTS AND DISCUSSION

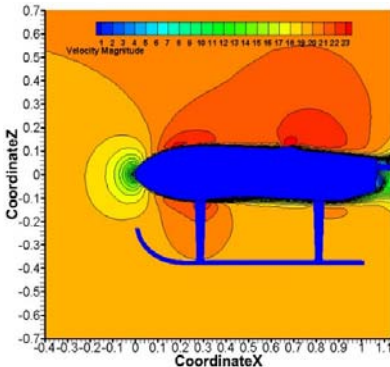
### A. The numerical simulation results of gas-phase

The convergent numerical simulation results were processed by the post-processing software called Tecplot, because it can display pressure and velocity contours more clearly than FLUENT.

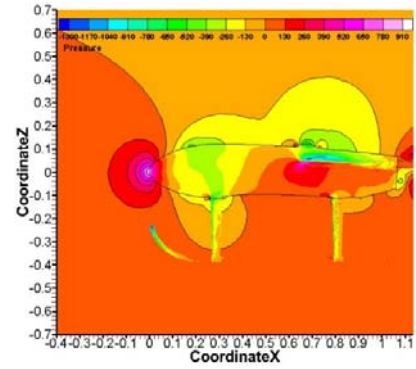
The optimal placement of the sampler should meet the following conditions: the pressure (P) is close to the operation pressure, the velocity (V) is approximately equal to the flight speed and airflow is smooth. Fig.2 illustrate the pressure distribution (a,c) and the mean streamwise (b,d) of the symmetry plane. These Figures show that both the bottom and the top of the fuselage meet the requirements. But for the UAV model used in the simulation, the parachute was installed on the top of the fuselage. So the top of fuselage was not suitable and only the bottom of the fuselage was studied in the following sections.



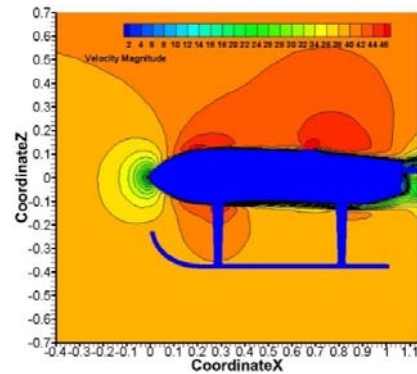
(a) Pressure at the speed of 20m/s



(b) Velocity at the speed of 20m/s



c) Pressure at the speed of 40m/s



d) Velocity at the speed of 40m/s

Fig.2: The pressure and velocity distribution of UAV fuselage and symmetry plane

The stable ranges of two flight speed are shown in table 1.

TABLE 1: DISTANCES OF STABLE P AND STABLE V FROM THE UAV NOSE/CM

| Flight speed | D1    | P(Pa) | D2    | V(m/s) | D3   | D4    |
|--------------|-------|-------|-------|--------|------|-------|
| 20 m/s       | 42~72 | 0~30  | 43~78 | 19~20  | 14.0 | 43~72 |
| 40 m/s       | 42~78 | 0~130 | 42~78 | 38~40  | 15.0 | 42~78 |

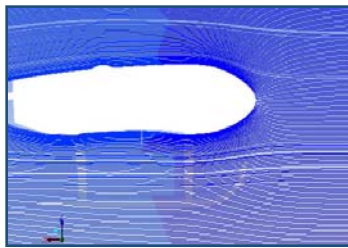
Note: The coordinates of the very front of the nose are (0, 0, 0); D1 is the distance of pressure stable region from the UAV nose; D2 is the distance of velocity stable range from the UAV nose; D3 is the largest vertical distance of stable velocity to X-axis; D4 is the distance of overlap region of pressure and velocity stable region from the nose.

From table 2, when the UAV fly at the speed of 20 m/s the aerosol sampler should be installed in the range of 43~72 cm from the UAV nose and the vertical distance from the X-axis is about 14.0 cm. When the flight speed is 40 m/s the distance from the UAV nose is 42~78 cm, the vertical distance from the X-axis is about 15.0 cm.

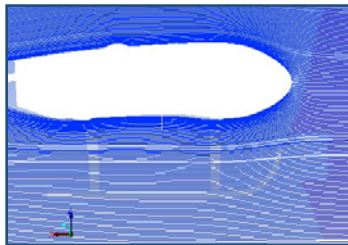
### B. The numerical simulation results of dispersed phase

Twohy. etal [9] proposed that particles trajectories may be affected as airflow streamlines are distorted by the outline of the aircraft. In general, very small aerosol particles approximately follow flow streamlines, while large aerosol particles tend to maintain their initial direction and speed. Intermediate-sized particles deviate from their initial

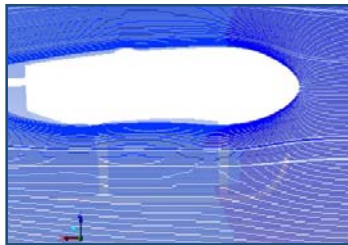
trajectories in the direction of, but not along the exact path, the streamlines. This leads to “shadow zones,” areas near the fuselage that are bypassed by trajectories of intermediate-sized droplets, and “enhancement regions,” areas outside of the shadow zones where the deflected trajectories converge. Particle concentrations are higher in enhancement regions than in the freestream, but are essentially zero in shadow zones. Fig.3 is the particle trajectories of different diameter at the speed of 40m/s.



(a) The trajectories of PM<sub>1</sub>



(b) The trajectories of PM<sub>2.5</sub>



(c) The trajectories of PM<sub>10</sub>

Fig. 3: The trajectories of different sizes of particles at the speed of 40 m/s

The particles trajectories under different speed are very similar, so this article only lists the figures of 40 m/s in Fig.3. Figures in Fig.3 show that: when PM<sub>1</sub> (a) and PM<sub>2.5</sub> (b) were released from the direction of velocity inlet at the same speed with the UAV, particles approximately followed the flow streamlines. While when PM<sub>10</sub> was released, particle trajectories changed significantly. The innermost particles deviated from the streamlines and biased toward the direction of gravity. Meanwhile the shadow zones became much more obvious than PM<sub>1</sub> and PM<sub>2.5</sub>. When the airflow streamlines were distorted by the outline of the UAV, the particles trajectories were also affected. And particles were converged on the areas outside the shadow zones. These results are the same as Twohy's.

Different diameters PM have different thickness of shadow zone plus enhancement region. Because the shadow zones of PM<sub>1</sub> and PM<sub>2.5</sub> were so thin that it was too difficult to get the accurate values via the manual measurement. According to the simulation results, the thickness of shadow zone of releasing PM<sub>10</sub> were about 0.8 cm and 1.5 cm for the flight speeds of 20 and 40m/s. The distances of homogeneous regions to X-axis of PM<sub>1</sub> and PM<sub>2.5</sub> were about 14.0 cm for 20m/s and 14.5 cm for 40m/s. For PM<sub>10</sub>, the distances were about 14.5cm and 15.0cm for 20 and 40m/s.

#### IV CONCLUSIONS

Combining the numerical simulation results of gas-phase and dispersed-phase, at the altitude of 600 m, when the UAV fly at the speed of 20 m/s, the optimal placement of sampler is about 43~72 cm from the UAV nose, and the vertical distance from the X-axis must exceed 14.5 cm. As the speed increases to 40 m/s, the optimal placement range become 42~78 cm from the UAV nose and 15.0 cm from X-axis. Finally, based on all the simulations above, the optimal placement of the sampler was about 43~72 cm from the UAV nose, and the vertical distance from the X-axis must exceed 15.0 cm. More experiments should be operated to determine the specific optimal placement of the sampler on the UAV according to the simulating results in the future.

#### REFERENCES

- [1] Chaloulakou, A., Kassomenos, P., Spyrellis, N., et al, Measurements of PM10 and PM2.5 particle concentrations in Athens, Greece. *Atmospheric Environment*, vol.37, pp. 649-660, 2003.
- [2] Sasaki, K., & Sakamoto, K., Vertical differences in the composition of PM10 and PM2.5 in the urban atmosphere of Osaka, Japan. *Atmospheric Environment*, vol.39, pp. 7240-7250, 2005.
- [3] Tominaga, Y., & Stathopoulos, T., CFD simulation of near-field pollutant dispersion in the urban environment: A review of current modeling techniques, *Atmospheric Environment*, vol.79, pp.716-730, 2013.
- [4] Gousseau, P., Blocken, B., Stathopoulos, T., et al, CFD simulation of near-field pollutant dispersion on a high-resolution grid: A case study by LES and RANS for a building group in downtown Montreal. *Atmospheric Environment*, vol.45, pp.428-438, 2011.
- [5] Nakahashi, K., Aeronautical CFD in the age of Petaflops-scale computing: From unstructured to Cartesian meshes. *European Journal of Mechanics - B/Fluids*, vol.40, pp.75-86, 2013.
- [6] Afroz, F., & Sharif, M. A. R., Numerical study of heat transfer from an isothermally heated flat surface due to turbulent twin oblique confined slot-jet impingement. *International Journal of Thermal Sciences*, vol.74, pp.1-13, 2013.
- [7] Cachon, B. F., Firmin, S., Verdin, A., et al, Inflammatory effects on human lung epithelial cells after exposure to diesel exhaust micron sub particles (PM1.0) and pollen allergens. *Environmental Pollution*, vol.161, pp.64-69, 2012.
- [8] Satsangi, P. G., Yadav, S., Pipal, A. S., et al, Characteristics of trace metals in fine (PM2.5) and inhalable (PM10) particles and its health risk assessment along with in-silico approach in indoor environment of India. *Atmospheric Environment*, vol.92, pp.384-393, 2014.
- [9] Twohy, C., & Rogers, D., Airflow and water-drop trajectories at instrument sampling points around the Beechcraft King Air and Lockheed Electra. *Journal of Atmospheric and Oceanic Technology*, vol.10, pp.566-578, 1993.